EGTRIB Journal
JOURNAL OF
THE EGYPTIAN SOCIETY OF TRIBOLOGY
VOLUME 22, No. 4, October 2025, pp. 20 - 34 **ISSN 2090 - 5882**
(Received June 28. 2025, Accepted in final form September 03. 2025) **jest.journals.ekb.eg**

APPLICATION OF TRIBOELECTRIC NANOGENERATOR TO CONTROL DOOR LOCK

Zeinab A. H.[1], Al-Kabbany A. M.[1,2] and Ali W. Y.[1]

[1]Production Engineering and Mechanical Design Dept., Faculty of Engineering, Minia University, El-Minia, EGYPT.
[2]Smart Biomaterials and Bioelectronics Lab, National Taiwan University, TAIWAN.

ABSTRACT.
The present paper aims to utilize a Triboelectric nanogenerator as a push-button to generate an electrical signal when a human finger presses a TENG button, thereby controlling a door lock. It is an application designed to help disabled and elderly individuals and enhance their level of comfort. For example, if the room has a controlled door-opening system, they can open the door without getting out of their seat. This ensures safety and reduces physical strain.

The present work demonstrates a triboelectric nanogenerator (TENG) of simple structure, a wide choice of materials, and low cost. Kapton, which provides a maximum voltage of 0.08 V, a maximum current of 35 nA, and a maximum power of 0.06 nW at an optimum resistance of 0.5 MΩ, is used to generate a signal by touch. The signal is then transmitted to the servo motor using an IR sensor, which turns and opens the door. This system highlights the potential of TENG-based interfaces for smart home applications, offering simplicity, safety, improved user accessibility, and opens the door for future research to power the application itself using the generated energy.

KEYWORDS
Triboelectrification, Kapton, corn husk, nylon, polyester, polytetrafluoroethylene, polypropylene, infrared ray sensor, remote control, and smart home.

INTRODUCTION

Mechanical energy harvested from human body movements is one of the most common and abundant energy sources available, with the significant advantage of being independent of time and location compared to other environmental sources. This energy can be captured, transformed into electricity, and stored for future use through transducer mechanisms such as triboelectric and piezoelectric nanogenerators, [1]. The core principle behind triboelectric nanogenerators (TENGs) is triboelectrification, [2, 3], a contact-induced electrification phenomenon that also enables self-driven sensing and blue energy harvesting. Furthermore, TENG-based

sensors have demonstrated excellent flexibility in applications ranging from environmental monitoring, [5] and human health monitoring, [4, 6] to motion detection, [7]. The triboelectric effect occurs when two materials come into contact through friction and become electrically charged. It is a common cause of daily electrostatic phenomena, [8 - 10]. The sign of the charges a material carries depends on its relative polarity to the material it contacts. This effect, likely understood for thousands of years, still has its underlying mechanism under investigation. The prevailing theory is that upon contact, adhesion occurs between surface atoms, forming chemical bonds. To equalize the electrochemical potential, charges, which may be electrons or ions, are transferred from one material to the other. Upon separation, some atoms retain extra electrons while others lose them, resulting in triboelectric charges on the surfaces. Materials with strong triboelectrification effects are typically insulators or poor conductors, allowing them to retain transferred charges for extended periods, [11, 12]. While the electron transfer model is well-understood for metals, based on differences in work functions, [13 - 15], the ion transfer model is considered more accurate for polymers and materials forming covalent bonds upon contact, [11, 12]. Figure 1 illustrates these two charge transfer mechanisms.

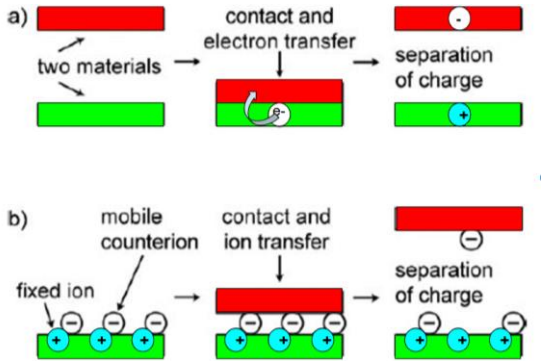

Fig. 1 Possible mechanisms of charge transfer, a) Transfer of an electron, b) Transfer of an ion.

The triboelectric effect occurs in almost all material types, including metals, polymers, wood, and silk. A material's ability to gain or lose electrons is determined by its position in the triboelectric series, [16]. When two materials from different positions in this series are brought into contact, the one higher up tends to lose electrons (becoming positively charged), while the one lower down tends to gain electrons (becoming negatively charged). The amount of charge transferred increases with the distance between the two materials in the series, [17]. A TENG is typically constructed by stacking two polymer sheets with significantly different triboelectric properties and coating the top and bottom of the structure with metal films. Due to nanoscale surface roughness, mechanical deformation causes friction between the films, generating equal but opposite charges on their surfaces. The resulting triboelectric potential at the interface acts as a charge "pump," driving electron flow in an external load when the system's capacitance changes, [18]. TENGs operate in several distinct modes of mechanical interaction. The vertical contact-separation

mode is the most widely adopted due to its simplicity and high-power density; it relies on two dielectric layers repeatedly touching and separating vertically to produce a potential difference, [21]. The lateral-sliding mode uses horizontal motion, such as sliding or rotating planar layers, to vary the contact area and generate alternating current, though it faces challenges from surface wear, [22]. In the single-electrode mode, a dielectric material interacts with a grounded electrode, with approach and separation driving electron flow to and from the ground, [19]. The freestanding triboelectric-layer mode involves a moving dielectric oscillating between two symmetrical electrodes, inducing electron flow without direct surface wear, [20]. Together, these modes illustrate the versatility of TENGs in converting mechanical energy into electrical power. While the theory behind TENG operation is well-established, performance in practical applications is highly material-dependent.

Therefore, this work systematically investigates the performance of six readily available triboelectric materials, such as polyimide (Kapton), polyamide 6-6 (nylon), polyester (PET), polytetrafluoroethylene (Teflon)(PTFE), polypropylene, and corn husk, for use as a touch-activated button in an assistive door lock control system.

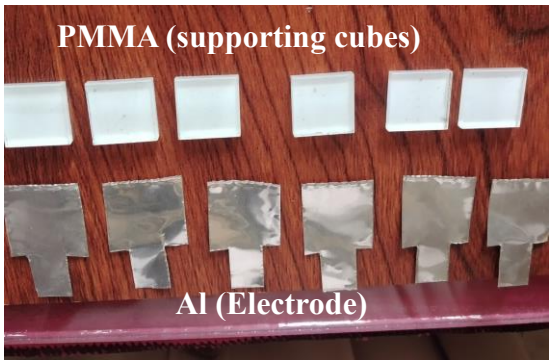

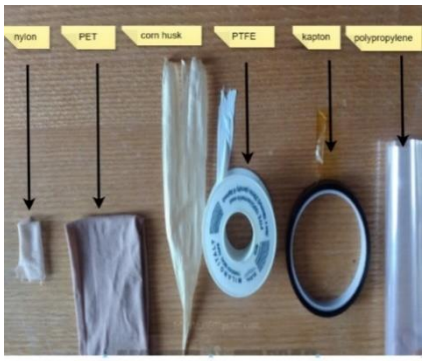

Fig. 2 a. The base of all buttons, b. The six triboelectric materials.

EXPERIMENTAL WORK

The six cubes of PMMA are used as the support for buttons, and the layers of the Aluminum foil with a thickness of 0.016mm were stuck with a double-face tape on all the buttons as the electrode, which is the primary collection of the button. Base button dimensions are 15*15*2.5 mm in Fig. 2 a. The triboelectric materials utilized in this experiment for interaction with the human finger include nylon, Kapton, corn husk, polyester, Teflon, and polypropylene, as shown in Fig. 2 b

The surface DC voltage (model SVM2) was used to determine the ESC between every pair of materials ,including the six materials and human skin. The device was placed approximately 20 mm after the two materials were brought into contact. the triboelectric series in Fig. 3.

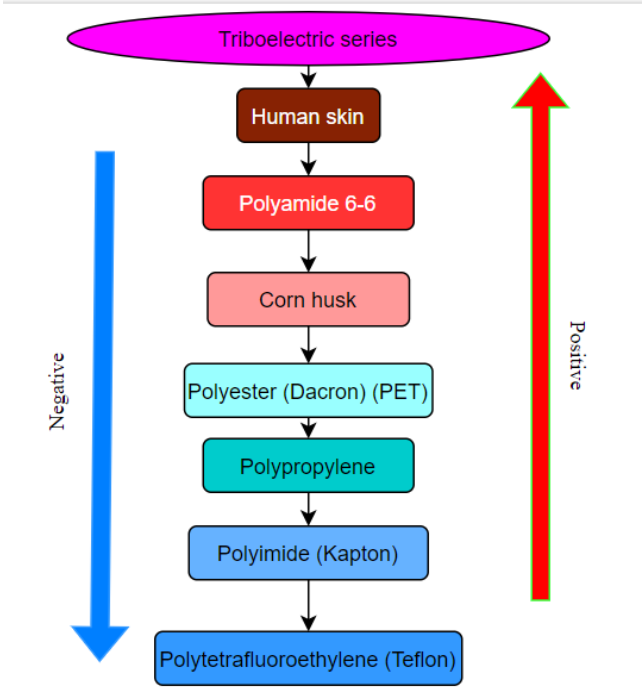

Fig. 3 Triboelectric series for the test materials.

The voltage was measured by using a Uni-T UT33A+ digital multimeter, and the device has a load cell to determine the effect of the normal load on the voltage at room temperature. the buttons were covered with a polymer to isolate them from environmental fluctuations during testing, Fig. 4.

The buttons were connected to the Arduino board, measuring the voltage. It is more accurate using the Arduino, compared to a standard multimeter. The button that produced the highest voltage was selected for integration with an infrared (IR) transmitter. Upon contact with the human finger, the IR signal is sent to the receiver, triggering a servo motor to rotate and open the door via programmed control. The underlying mechanism relies on triboelectric interaction: when the human finger touches the substrate material, free electrons transfer from the skin (which loses electrons) to the dielectric surface (which gains electrons and becomes negatively charged). Upon separation, a positive charge is induced on the electrode, opposite in polarity to the material's charge, as illustrated in Fig. 5. This dynamic generates an electric current that can be harnessed for actuation.

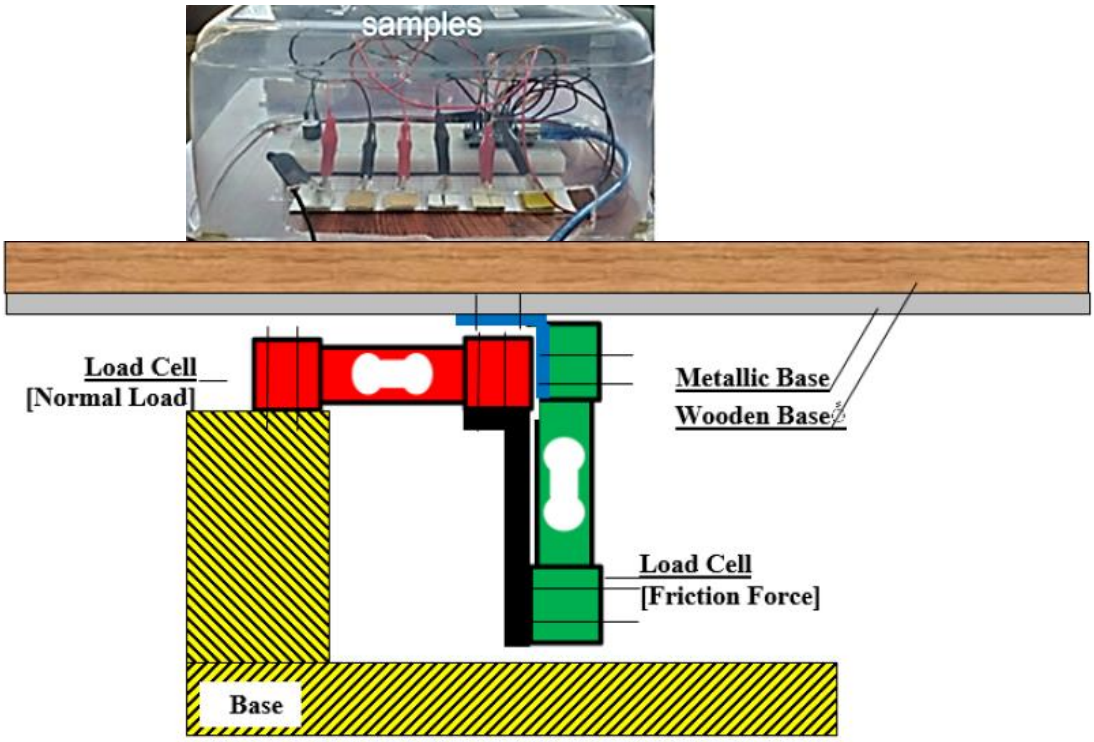

Fig. 4. Device for measuring the normal load of human finger during recording voltage for every button, [23].

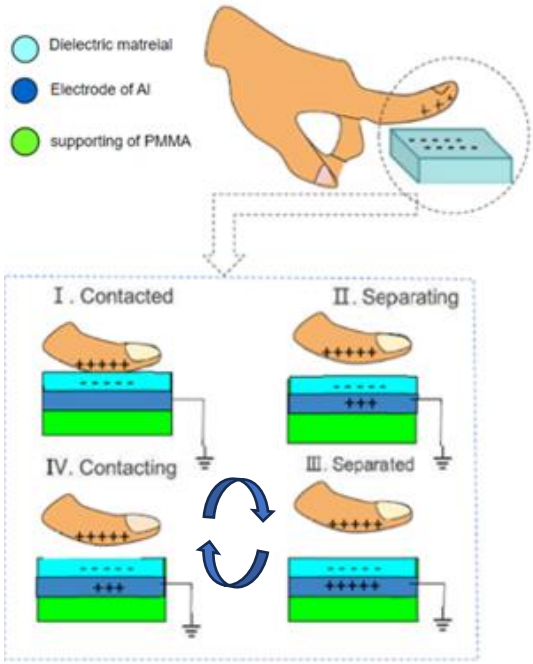

Fig. 5. Generation of ESC on contacted surfaces.

Three buttons, Kapton, corn husk, and PTFE, were selected and connected to a circuit with external resistances ranging from 0.33 to 65 MΩ, as shown in Fig. 6, to evaluate the current and power output of each button. The corresponding results are presented in Figs. 13-18.

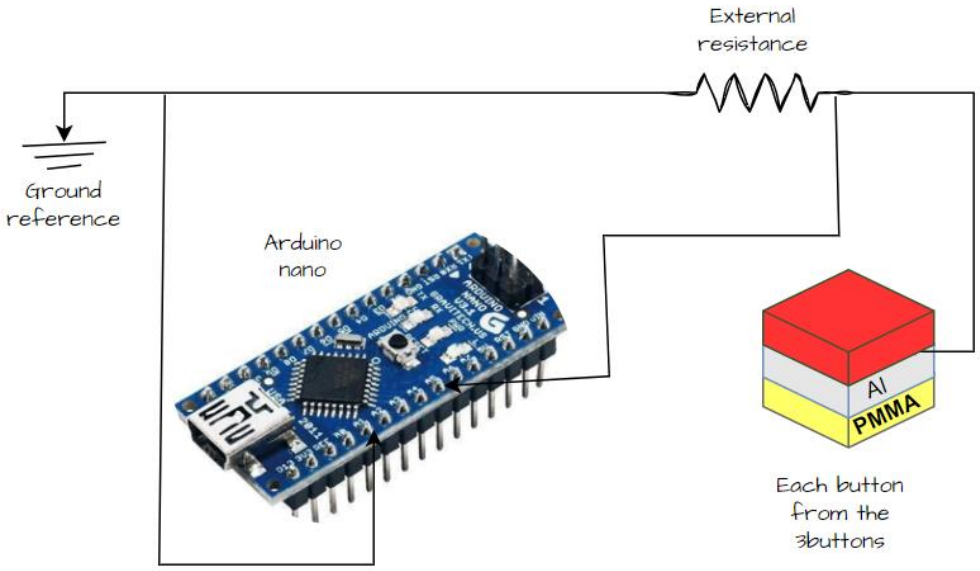

Fig. 6 Test setup for a single button when connecting with external resistance.

RESULTS AND DISCUSSION

A comparison was made between the outputs of the six buttons to identify the one with the highest electrical voltage. It was found that Kapton had the highest voltage, followed by corn husk, and then Teflon, Fig. 7.

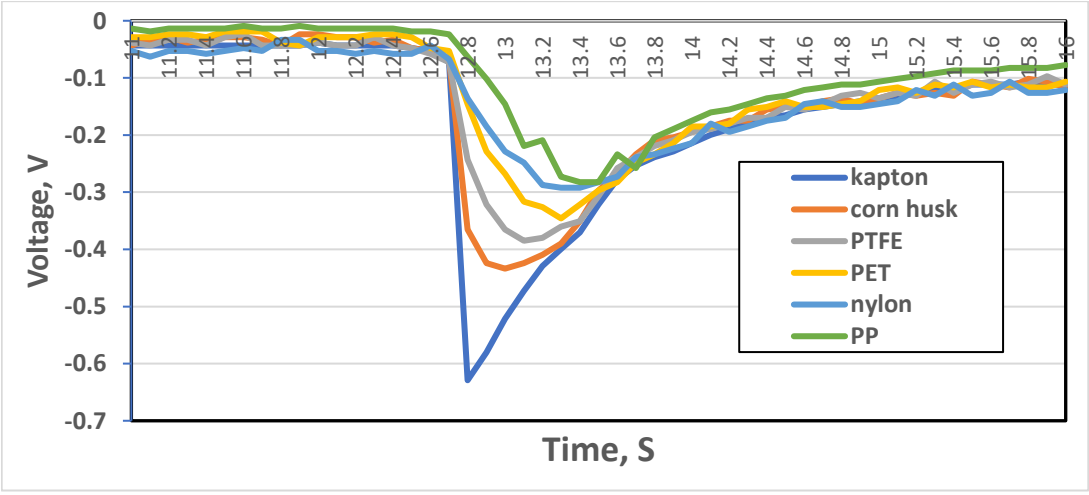

Fig. 7 The effect of pressing one button on the other 5 buttons of the Arduino reading.

Additionally, when the Kapton, corn husk, and PTFE exhibit high voltage values, the voltage of the three buttons was measured under varying finger forces, which represented a range of 1 to 14 N, and the results are shown in Figs. 8-10.
According to the triboelectric series the three materials of the buttons are below the human skin so, the charge which generated by the contact-separation is negative.

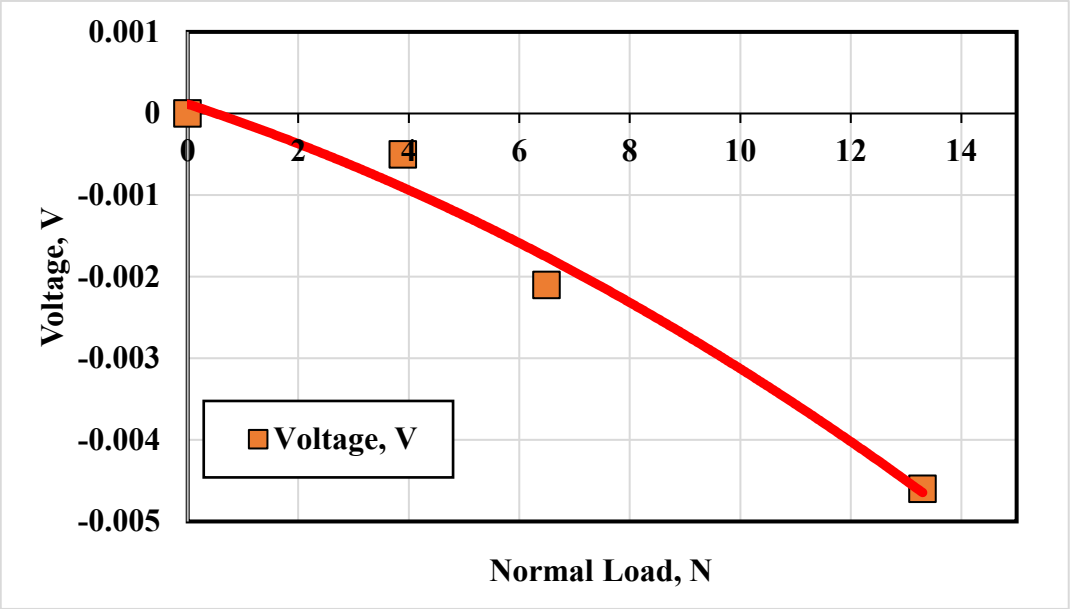

Fig. 8 The relation between the human finger force and the button output voltage of corn husk.

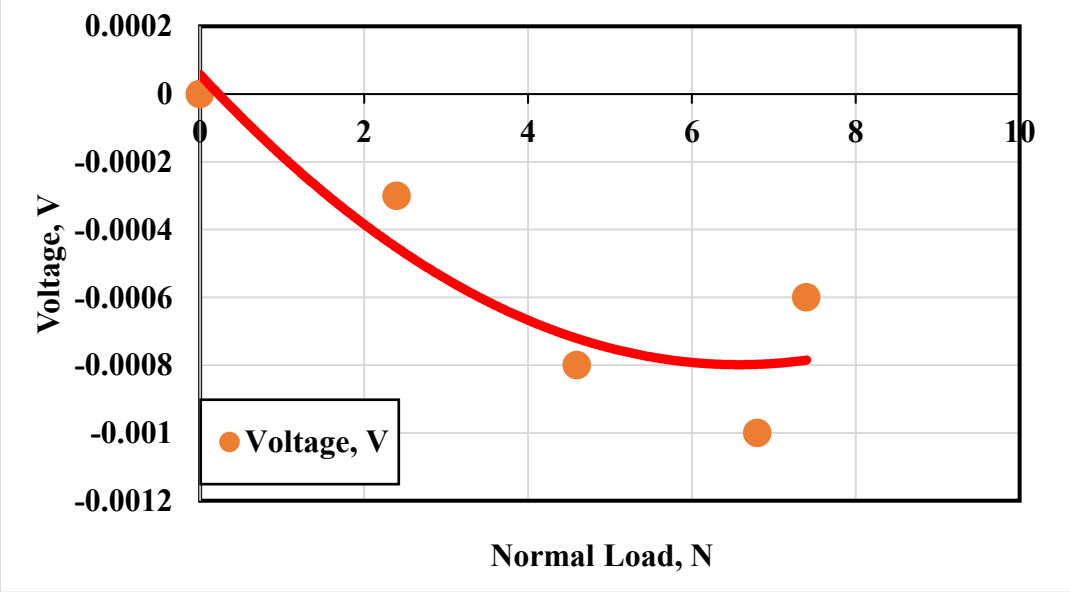

Fig. 9 The relation between the human finger force and button output voltage of PTFE.

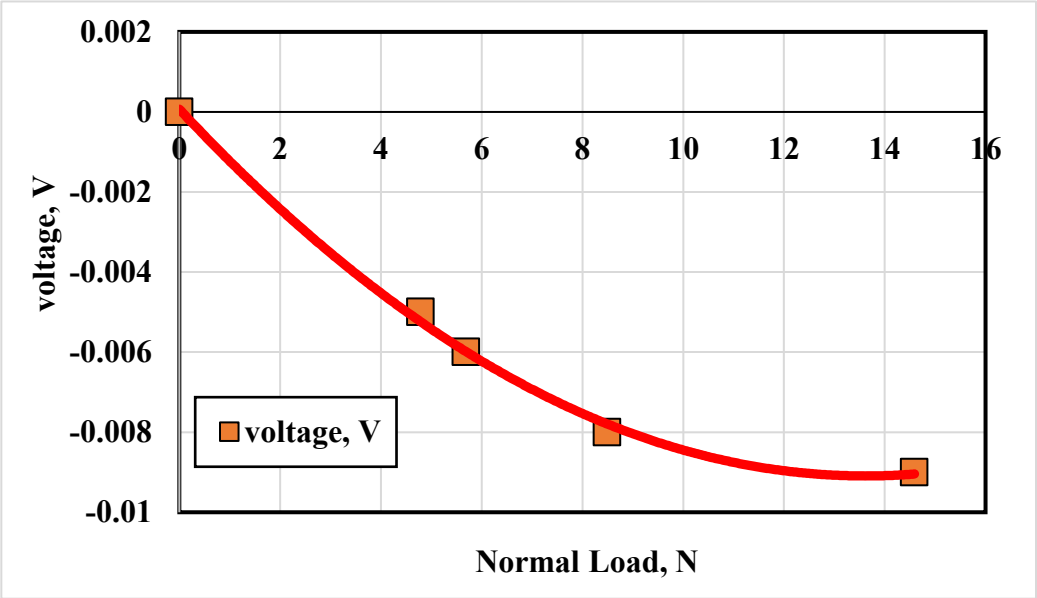

Fig. 10 The relation between the human finger force and the button output voltage of Kapton.

In general, the voltage increased by increasing the normal load on every button, but the value at the same load differs from one material to another. At the load of 6 N in the PTFE curve, the maximum voltage was 0.008V, at the same load of the Kapton and corn husk in Figs. 8,10, the maximum voltages were 0.006V and 0.002V, respectively.

Although PTFE was positioned at the bottom of the triboelectric series, the experimental results demonstrated that Kapton generates a higher voltage; this discrepancy may be attributed to the surface characteristics of PTFE, which tend to adhere to the opposing surface, potentially affecting charge transfer efficiency.

Due to the ability of the Kapton material to generate a higher voltage, a Kapton button was used to provide the lock with the signal for opening and closing as an alternative to the remote control, as shown in Figs. 11, 12. However, efforts are still ongoing to make it a self-powered application.

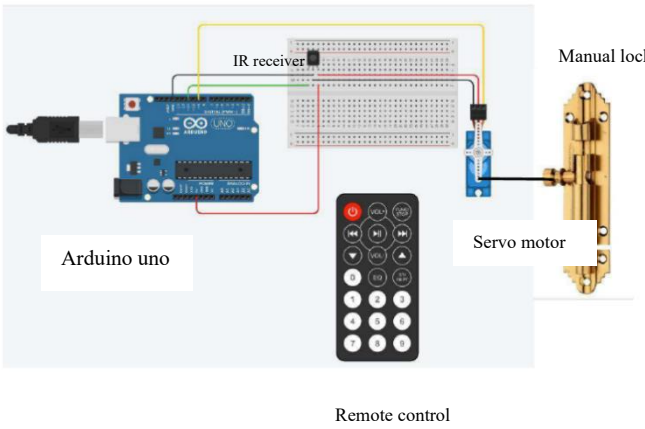

Fig. 11 Complete system using remote control [https://www.tinkercad.com/ +google drawing]

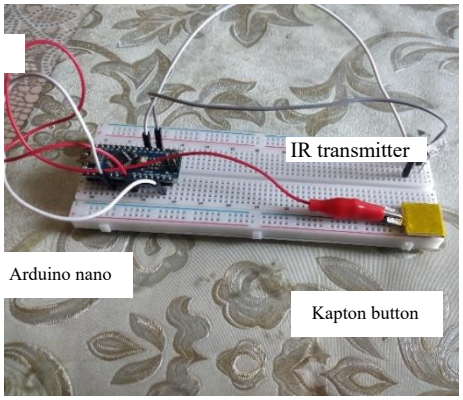

Fig. 12 The setup of the Kapton button with the IR sensor (alternative remote control).

When a TENG is connected to a resistive load as shown in Fig. 6, its operation can be divided into three regions based on the load resistance. At low resistance, the voltage increases approximately proportionally with resistance while the current decreases slightly; at an intermediate resistance, voltage and current intersect, representing the optimal load where maximum instantaneous power is delivered; and at high resistance, the voltage saturates near the open-circuit voltage and the current drops significantly. The intermediate region is crucial for achieving maximum power output and is therefore important for optimizing the TENG's performance. Figs. 13-18 shows the optimum resistance and maximum power for the 3 buttons: Kapton, corn husk, and PTFE.

For Kapton, the voltage and current data shown in Fig. 13 indicate that the output voltage increases with increasing external resistance, reaching a maximum of 0.08 V at 50 MΩ. Conversely, the current decreases as resistance increases, with a peak current of 35 nA observed at 0.5 MΩ. In Fig. 14, the power curve shows two distinct regions of TENG operation: an intermediate region and a third region where the power drops from its maximum value of 0.06 nW at 0.5 MΩ to zero at the open-circuit voltage.

For corn husk, the voltage and current data shown in Fig. 15 indicate that the output voltage increases with increasing external resistance, reaching a maximum of 0.03 V at 55 MΩ. Conversely, the current decreases as resistance increases, with a peak current of 49.3 nA observed at 0.33 MΩ. In Fig. 16, the power curve shows two distinct regions of TENG operation: an intermediate region and a third region where the power drops from its maximum value of 0.08 nW at 0.33MΩ to zero at the open-circuit voltage.

For PTFE, the voltage and current, Fig. 17, indicate that the output voltage increases with increasing external resistance, reaching a maximum of 0.02 V at 55 MΩ.

Conversely, the current decreases as resistance increases, with a peak current of 49 nA observed at 0.33 MΩ. In Fig. 18, the power curve shows two distinct regions of TENG operation: an intermediate region and a third region where the power drops from its maximum value of 0. 08 nW at 0.33 MΩ to zero at the open-circuit voltage.

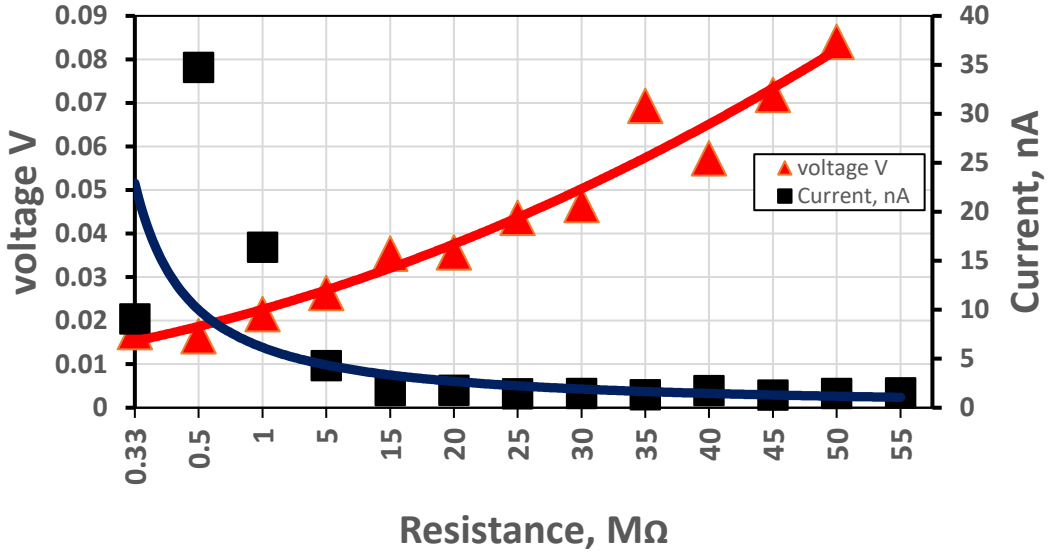

Fig. 13 Effect of the external resistance on the voltage and current output of the Kapton button.

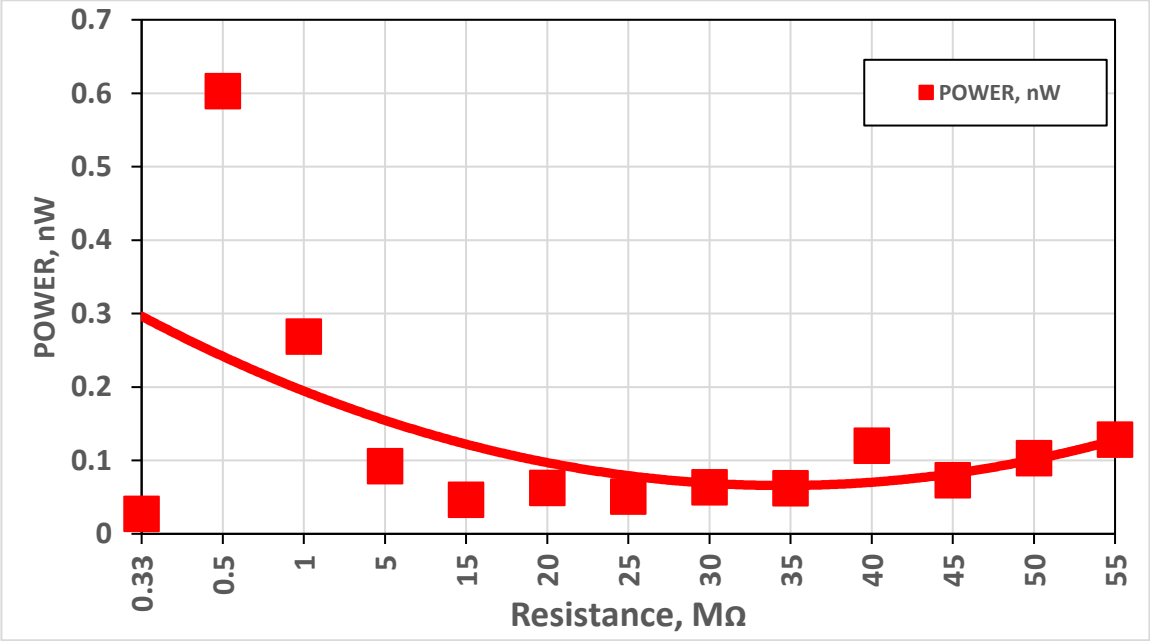

Fig. 14 Effect of external resistance on the power output of the Kapton button.

Fig. 15 Effect of the external resistance on the voltage and current output of the corn husk button

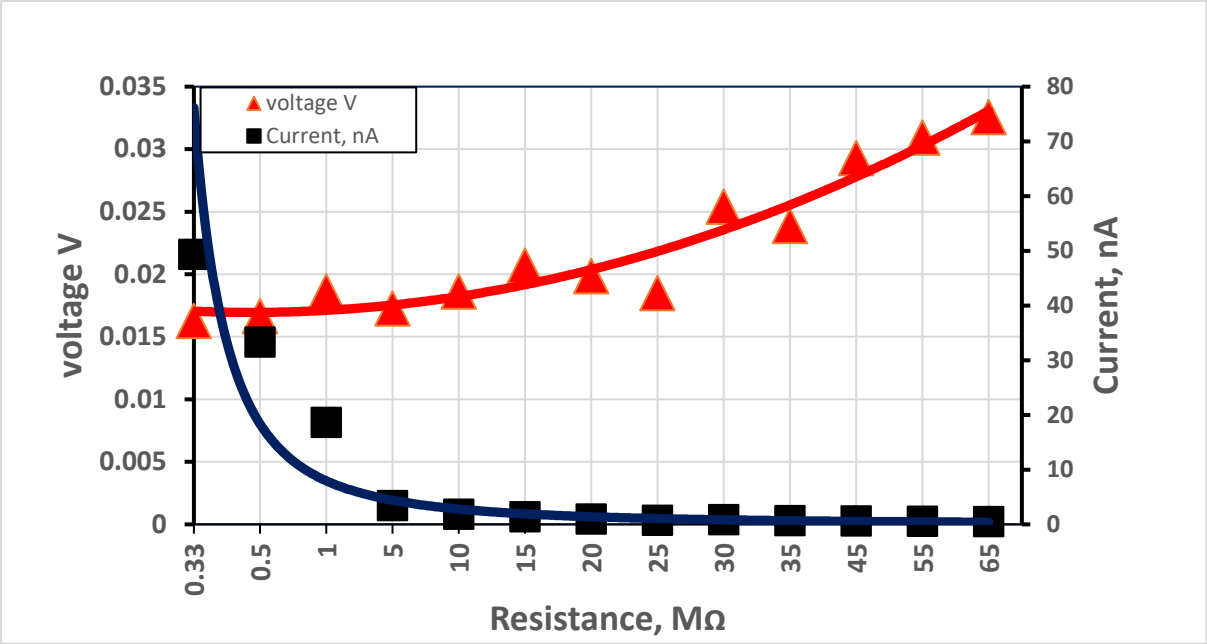

Fig. 15 Effect of the external resistance on the voltage and current output of the corn husk button.

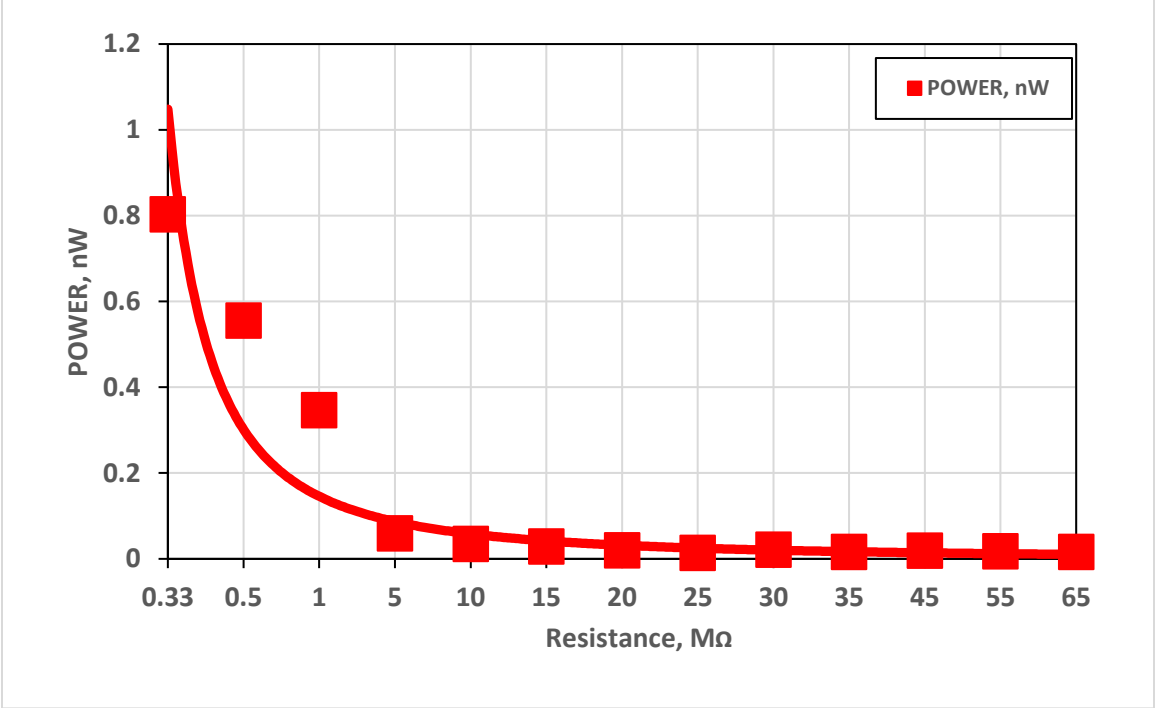

Fig. 16 Effect of external resistance on the power output of the corn husk button.

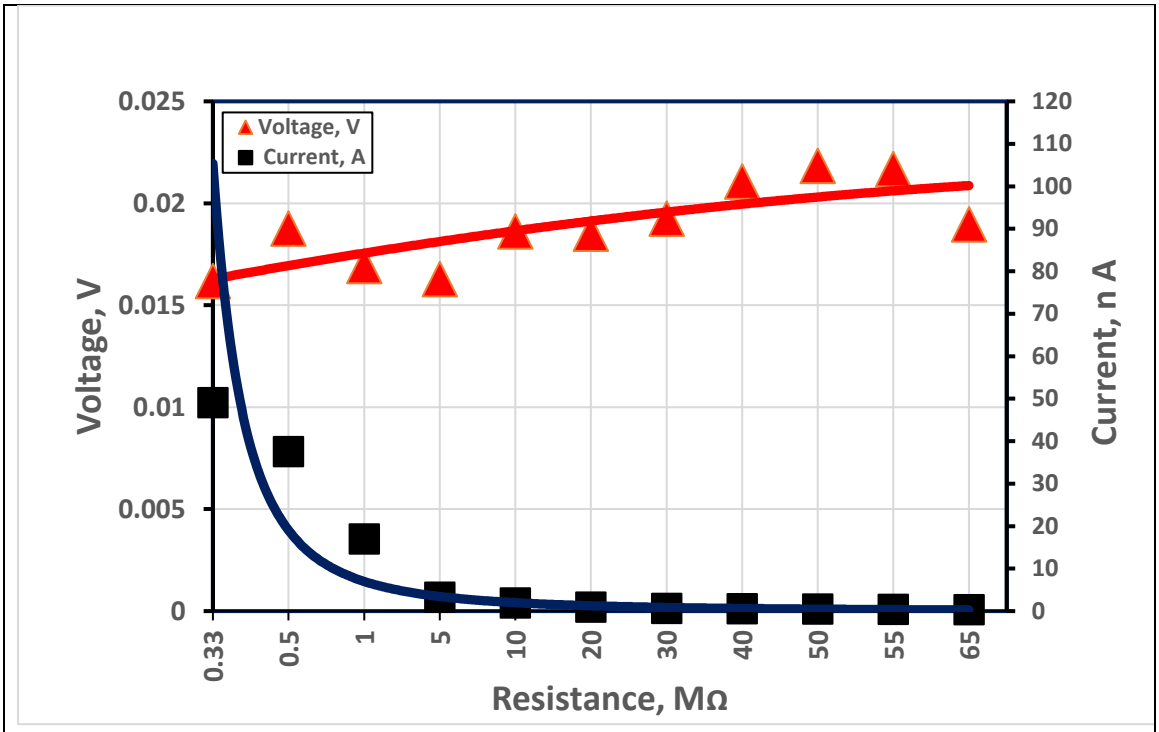

Fig. 17 Effect of the external resistance on the voltage and current output of PTFE

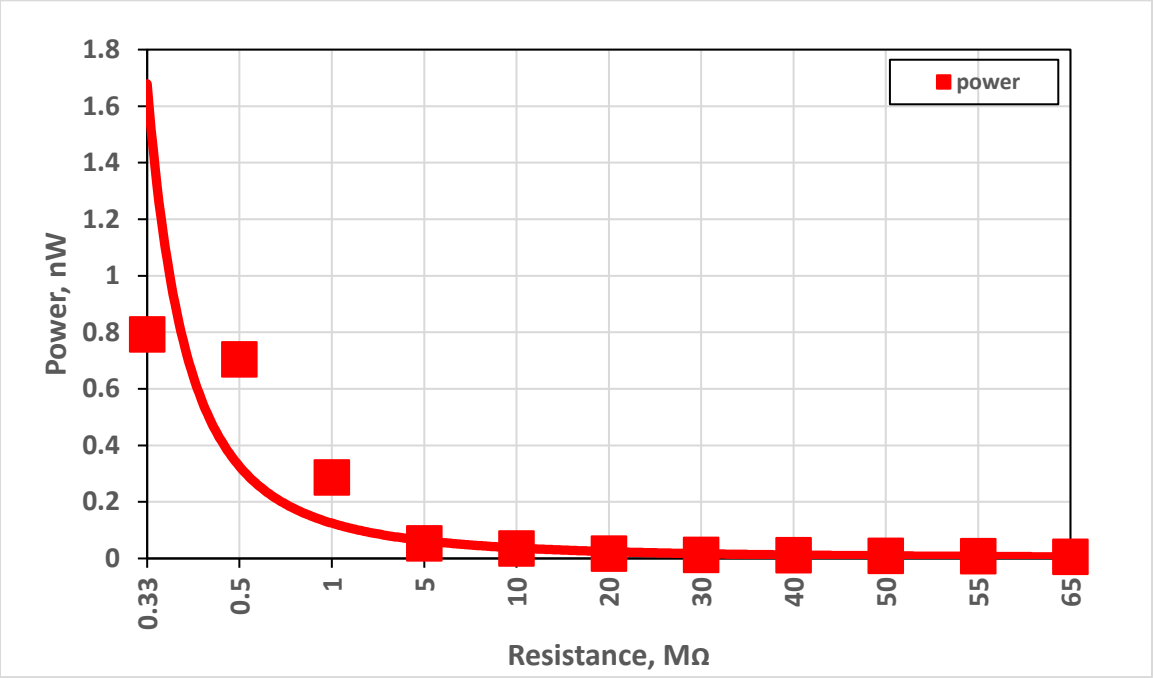

Fig. 18 Effect of external resistance on the power output of the PTFE button.

When the TENGs (Kapton, Teflon, and corn husk) are connected to resistance from 0.33 MΩ to 65 MΩ. It was found that the voltage and current curves intersect at a point, and the resistance is called the optimum resistance. The optimum resistance for Kapton was 0.5 MΩ in Fig. 13 and gives a maximum power of 0.6 nW in Fig. 14. For corn husk and the PTFE, the optimum resistance is 0.33MΩ in Figs. 15, 17, which gives a power of 0.8 nW in Figs. 16, 18, respectively. The optimum resistance that would provide maximum power for the TENG, [24], which maximizes the TENG efficiency in case of charging capacities.

CONCLUSIONS

1. The present work aims to assist elderly people in performing daily tasks at home, such as opening doors, switching on lights, and controlling objects.

2. Among the tested materials, Kapton exhibited the highest voltage, making it suitable for control applications. Meanwhile, corn husk produced the highest current and power, enabling energy storage in capacitors to supply the circuit with the necessary power, potentially replacing batteries, which are costly and environmentally harmful.

3. The characteristics of PTFE (Teflon) tend to adhere to the opposing surface, potentially affecting charge transfer efficiency, which was demonstrated by the lowest outputs compared to Kapton.

4. The selected TENG materials are affordable and readily available.

The next phase of this work will focus on integrating these optimized TENG materials into a functional, user-friendly prototype system for real-home environments. Future research will also explore the scalability of the energy harvesting units and the long-term durability of the materials under continuous use.

REFERENCES

1. Gol\kabek J. and Strankowski M., "A review of recent advances in human-motion energy harvesting nanogenerators, self-powering smart sensors and self-charging electronics," *Sensors*, vol. 24, no. 4, p. 1069, (2024).

2. Al-Kabbany A. M., Zeinab. A. H., and Ali W. Y., "Development of a Chess Board With Self-Powered Move Recognition," *J. Egypt. Soc. Tribol.*, vol. 21, no. 3, pp. 96–105, (2024).

3. Jian L., S. Yang, J. Wang, and Hua M., "Triboelectrification electrostatic potential of MC nylon 6 under point contact dry sliding," *Tribol. Lett.*, vol. 36, no. 3, pp. 199–208, (2009) ,

4. Ali A. S., Zeinab A. H., Al-Kabbany A. M., and Ali W. Y., "ARM ROTATING SENSOR BASED ON TRIBOELECTRIC NANOGENERATOR," *J. Egypt. Soc. Tribol.,* pp. 61–70, (2025).

5. M. K. Sharma *et al.*, "Self-powered AlGaN/GaN HEMT-based sensor integrated with rotational TENG for comprehensive water quality analysis," *Nano Energy*, vol. 135, p. 110637, Mar. (2025).

6. P. Parashar *et al.*, "Machine learning-driven gait-assisted self-powered wearable sensing: a triboelectric nanogenerator-based advanced healthcare monitoring," *J. Mater. Chem. A*, vol. 13, no. 19, pp. 13750–13762, May (2025)

7. P. Parashar *et al.*, "A Highly Flexible Self-Powered Triboelectric Sensor Array for Silent Speech Recognition and Swallowing Motion Analysis," *Small*, p. 2503969, (2025)

8. Horn R. G. and Smith D. T., "Contact electrification and adhesion between dissimilar materials," *Science (80-).*, vol. 256, no. 5055, pp. 362–364, (1992).

9. Willatzen M., and Wang Z. L., "Contact electrification by quantum-mechanical tunneling," *Research*, vol. 2019, p. 6528689, Jan. (2019),

10. Apodaca M. M., Wesson P. J., Bishop K. J. M., Ratner M. A., and Grzybowski B. A. , "Contact electrification between identical materials," *Angew. Chem., Int. Ed.*, vol. 49, no. 5, pp. 946–949, Jan. (2010).

11. McCarty L. S. and Whitesides G. M., "Electrostatic charging due to separation of ions at interfaces: Contact electrification of ionic electrets," *Angew. Chemie - Int. Ed.*, vol. 47, no. 12, pp. 2188–2207, (2008).

12. Diaz A. F., Wollmann D., and Dreblow D., "Contact electrification: ion transfer to metals and polymers," *Chem. Mater.*, vol. 3, no. 6, pp. 997–999, Nov. (1991).

13. Zhao X. *et al.*, "Studying of contact electrification and electron transfer at liquid–

liquid interface," *Nano Energy*, vol. 87, p. 106191, Sep. (2021)

14. Lin S., Xu L., Chi Wang A., and Wang Z. L., "Quantifying electron-transfer in liquid–solid contact electrification and the formation of electric double-layer," *Nat. Commun.*, vol. 11, no. 1, pp. 1–8, Dec. (2020).

15. Lin S., Xu L., Zhu L., Chen X., and Wang Z. L., "Electron transfer in nanoscale contact electrification: photon excitation effect," *Adv. Mater.*, vol. 31, no. 27, p. 1901418, Jul. 2019,

16. Zhang C. and Wang Z. L. , "*Triboelectric Nanogenerators*". . doi: 10.1007/978-981-10-5945-2_38, (2018).

17. Seol M. *et al.*, "Triboelectric series of 2D layered materials," *Adv. Mater.*, vol. 30, no. 39, p. 1801210, Sep. (2018).

18. Fan F. R. , Tian Z. Q. , and Wang Z. L , "Flexible triboelectric generator," *Nano Energy*, vol. 1, no. 2, pp. 328–334, Mar. (2012).

19. Al-Kabbany A. M., "Characteristics of a Kapton triboelectric nanogenerator-based touch button's voltage output," *Nano Energy*, vol. 114, no. June, p. 108620, (2023).

20. Ibrahem R. A., "Performance Evaluation of Free-Standing Triboelectric Generator (F-S Teg) Using Different Electrodes and Triboelectric Layers," *J. Egypt. Soc. Tribol.*, vol. 21, no. 1, pp. 53–61, (2024)

21. Kumar R., Goyal A. K., and Massoud Y., "Performance optimization of contact-separation mode triboelectric nanogenerator using dielectric nanograting," *Results Eng.*, vol. 22, no. April, p. 102-108, (2024).

22. Song W. Z. *et al.*, "Sliding mode direct current triboelectric nanogenerators," *Nano Energy*, vol. 90, no. PA, p. 106531, .(2021).

23. Eyad M. A., Al-Kabbany A. M., Youssef M. M., Ali W. Y., and Ali A. S. "PROPER SELECTION OF FLOOR MATERIALS IN HOSPITALS". *Journal of the Egyptian Society of Tribology*, *21*(4), 1-13,(2024).

24. Rashed A., Al-Kabbany A. M., Zeinab A. H., Youness K. A. and Ali W. Y. , "WIND SPEED SENSOR BASED ON SLIDING TRIBOELECTRIC,"*J. Egypt. Soc. Tribol.,* pp. 106–116, (2023).